Crystal Size Dependent Flexibility in ZIF-7: From Macro- to Nano-Scale

Rimita Bose,[†¥] Volodymyr Bon,[‡] Nadine Bönisch,[‡] Parasuraman Selvam,[§ ¥] Niket S. Kaisare[†], Stefan Kaskel,[‡*]*

[†]Department of Chemical Engineering, Indian Institute of Technology Madras, Chennai 600036, India

[‡]Department of Inorganic Chemistry I, Technische Universität Dresden, Bergstr. 66, D-01069, Germany

[§]Department of Chemistry, Indian Institute of Technology Madras, Chennai 600036, India

[¥]National Centre for Catalysis Research (NCCR), Indian Institute of Technology Madras, Chennai 600036, India

ABSTRACT

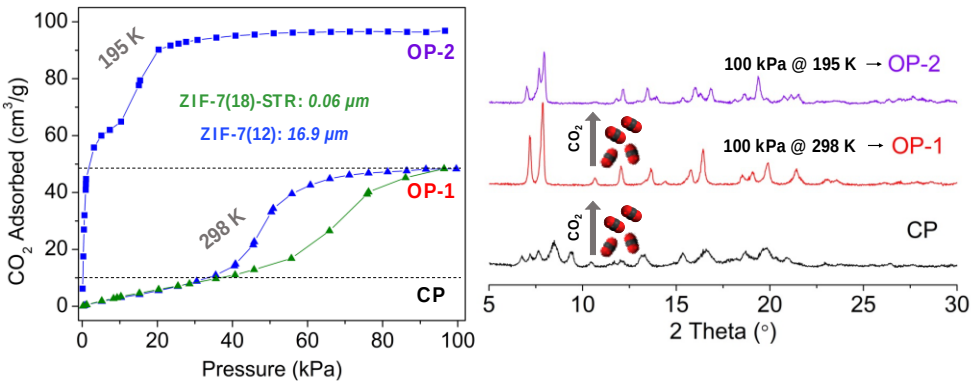

Flexible metal-organic frameworks (MOFs) are highly desirable materials for gas separation but most of them become rigid when the particle size is reduced towards nanoscale. We aim to comprehend the effect of textural properties such as crystal size, its distribution and morphology on the gate-opening behaviour stimulated by adsorption of guest molecules in ZIF-

7. The synthesis conditions are varied to obtain ZIF-7 batches with crystal sizes ranging between 0.05 and 15 μm with various size distributions. We report for the first time a CO_2-filled open pore phase of ZIF-7 at 195 K (OP2) derived from *in situ* powder X-ray diffraction (PXRD) data measured in parallel to CO_2 physisorption. The adsorption of CO_2 on ZIF-7 indicates persisting flexibility for all particle size regimes; with the crystal size, its distribution and morphology having a significant impact on both gate-opening and gate-closing pressures and slope of CO_2 adsorption isotherms. *In situ* PXRD measurement indicated further expansion of ZIF-7 framework in presence of methanol as guest species. The capability of ZIF-7 to accommodate molecules larger than its 0.3 nm window diameter signifies the importance of intermolecular interactions to overcome the energy barrier for linker movement/gating of the framework.

INTRODUCTION

Since the discovery of metal-organic frameworks (MOFs),[1] they have shown potential for multiple applications such as adsorption and separation, heterogeneous catalysis, sensing, biological and medical applications etc.[2,3] MOFs are crystallized by self-assembly of metal ions or clusters with multi-dentate organic linkers under suitable conditions. Owing to these extended bonds between metal and organic moiety, several MOFs possess stimuli-induced framework flexibility, which is an outstanding property of this class of solids. Kitagawa *et al.* have coined these materials as 'soft porous crystals', which retain their structural integrity while undergoing phase transformation in response to external stimuli.[4]

The flexibility in MOFs can be triggered by external stimuli such as mechanical pressure, temperature or adsorption of guest molecules. Various mechanisms of flexibility such as linker rotation, breathing, swelling, and subnetwork displacement[5] have been reported. Tanaka *et al.* have explained the linker rotation of ZIF-8 results in gating phenomenon, where the crystallographic information is retained except for the expansion of unit cell edge; they showed

that the gating pressure shifts to higher value with increase in temperature owing to the change in activation energy barrier for ZIF-8 with Ar as adsorbate.[6] Breathing is a two-step transformation accompanied by the change in the crystal structure exhibited by MIL-53(M) series MOFs (M = Al, Fe, Cr, Sc, Ga).[7] Swelling is observed in MIL-88 series where the unit cell volume changes from 85% to 230% without affecting the crystallographic space group and unit cell angles.[8,9] Subnetwork displacement, which is a recent discovery, arises from the displacement between two interpenetrated net is observed in InOF-23.[10]

Flexible MOFs have been discussed for applications such as gas storage and separation, and producing threshold sensors and actuators. The "gate-opening" transition in Co(bdp)[11] and "breathing" phenomenon in MIL-53(Al)[12] results in enhanced working storage capacity than their rigid analogues. Tanaka and co-authors explored ELM-11 as efficient material for CO_2/CH_4 separation.[13] DUT-8(Ni) was proven to selectively open its pores for D_2 vs. H_2 resulting in efficient H_2/D_2 separation.[14] Kitagawa and co-workers showed the efficient separation of water isotopologues using dynamic aperture in the flexible MOF.[15] Flexible MOF/carbon composites can be used as an efficient *n*-butane threshold sensor.[16] MIL-53(Al) and DUT-49 have been tested as force and pressure amplifiers.[17,18]

This work explores guest-molecule-induced flexibility in zeolitic imidazolate frameworks (ZIFs),[19] a sub-family of MOFs known for their thermal and chemical stability. Several ZIFs exhibit structural flexibility, wherein they undergo dynamic changes on exposure to external stimuli.[20–27] ZIF-7, which is constructed of Zn ions and benzimidazolate ligands,[28] exhibits flexibility triggered by guest molecules such as CO_2. Aguado *et al.* were the first to report its reversible breathing behaviour and S-shape isotherm at different temperature and CO_2 partial pressure.[20] Zhao *et al.* reported the mechanism of ZIF-7 phase transition occurs through CO_2 migration.[29] Later this framework flexibility was explored for several other gases and vapours.[30–35] S-shaped isotherms are of practical interest for separation applications due to

better selectivity and higher working capacity during charging-discharging cycles in adsorbent bed.[13] ZIF-7 is interesting for CO_2 capture since it remains rigid with N_2 as guest[30], but shows an S-shaped isotherm triggered by CO_2 at 298 K and under 1 bar pressure. The ambient experimental conditions are in contrast with most MOFs that show flexibility under higher pressure or lower temperature closer to their boiling point.[36–39]

The crystal size dependent flexibility is observed for a large number of flexible MOFs.[42–44] It is now considered as a general trend in MOF chemistry, indicating rather flexible behaviour in macro-crystals and structural rigidity of nano-crystals.[45] The influence of crystal size on the flexibility of ZIF-8 was reported by Lively and co-workers, whereas Tian et al. studied the mechanism of structure transition by *in situ* powder X-ray diffraction (PXRD).[40,41] While most flexible MOFs typically become rigid[42,44,46–48] below 1 μm crystal size, but ZIF-7 crystals are unique in exhibiting structural flexibility at even 80 nm crystal size. In the light of the use of nano-crystals in membranes or thin film technology,[49] this study is focused on establishing a better understanding of flexibility owing to particle downsizing towards nanoscale.

To the best of our knowledge, this is a first comprehensive work analysing the effect of crystal size of ZIF-7 on its phase transition. We use solvothermal (static/non-stirring) and stirring (dynamic) synthesis to control nucleation and crystal growth to produce crystals of different sizes, morphology, and distribution. Further, two-step centrifugation is used to obtain two different crystal sizes (including nanocrystals) from the same batch and show that ZIF-7 maintains the flexible behaviour at nanoscale. The in-house *in situ* powder X-ray diffraction (PXRD) in parallel to gas/vapour physisorption is intended to expand our fundamental understanding of ZIF-7 flexibility and the importance of surface barrier on downsizing. Further CO_2 adsorption at 195 K reveals a new, hitherto unknown CO_2-adsorbed phase of ZIF-7. Adsorption of alcohols, heptane, and toluene provides insight into ZIF-7 framework expansion, emphasizing the importance of molecular interactions rather than the compatibility between

pore aperture and guest kinetic diameter. The significance of this work, therefore, lies in elucidating how the macroscopic properties of ZIF-7 may affect adsorption behaviour of ZIF-7, potentially enabling researchers to rationalize the crystal size to tune the adsorption behaviour[13] or to downsize the crystals without affecting flexibility for preparation of ZIF-7 composites, membranes, or thin films.[49]

EXPERIMENTAL SECTION

Chemicals

The chemicals used for ZIF-7 synthesis, zinc nitrate hexahydrate (reagent grade, 98%) and zinc acetate dihydrate (reagent grade, 98%) were bought from Sigma Aldrich, and the linker benzimidazole (HbIm) either from Sigma Aldrich or TCI (both 98% purity). Solvents dimethylformamide (DMF) and methanol of HPLC grade were purchased from Thermo Fischer Scientific. These chemicals were used without any further purification.

Synthesis of ZIF-7

We adapted the synthesis from Zhao et al.[29] and optimized to obtain > 1 g of ZIF-7 with a yield exceeding 70% for all the batches. We used solvothermal (static/non-stirring) and stirring (dynamic) methods with varying ligand concentration and temperature to synthesize phase pure open-pore ZIF-7 with different particle sizes.

Conventional Solvothermal (Static)

In the conventional solvothermal synthesis, 5 mmol (1.48 g) $Zn(NO_3)_2.6H_2O$ was dissolved in 350 mL of DMF, followed by addition of 10 mmol (1.18 g) of benzimidazole (HbIm) and stirred for 15 minutes. When the mixture started to become turbid, it was transferred to a Schott bottle and heated at 403 K for 48 h in an oven. The white precipitate was first separated by centrifugation from the mother liquor, then washed using fresh DMF by stirring overnight, centrifuged and then the solid was dried in an oven at 353 K for 2 days. This material is

abbreviated as ZIF-7(12) hereafter (12 signifies the Zn:HbIm molar ratio). The synthesis is schematically shown in Fig. 1.

We repeated the synthesis method with Zn:HbIm molar ratios of 1:4 (using 20 mmol or 2.36 g HbIm) and 1:8 (using 40 mmol or 4.72 g HbIm), with remaining procedure kept the same, to achieve particles of size smaller than 15 μm. These two batches are labelled as ZIF-7(14) and ZIF-7(18), respectively.

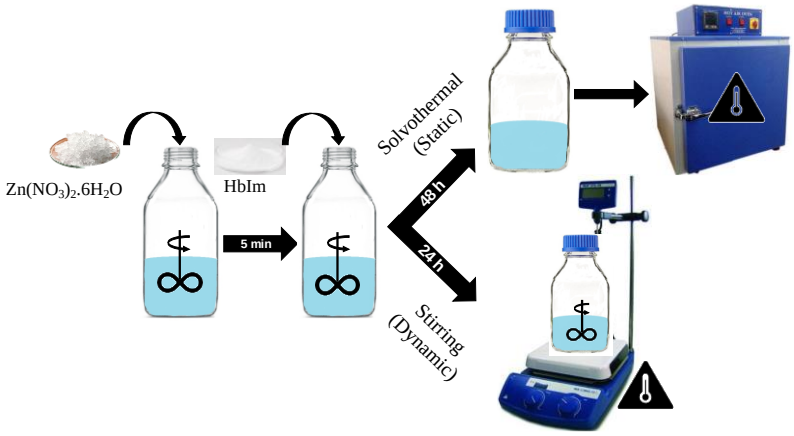

Figure 1: Pictorial representation of solvothermal and stirring-based synthesis approaches.

Solvothermal (Static): Two-step separation

Conventional solvothermal synthesis leads to a broader crystal size distribution. We used two-step centrifugation to separate micron and nano-size crystals synthesized in one-pot. As shown in Fig. 2, the solids were first separated using a lower RPM (larger sized crystals), followed by extraction of nano-sized ZIF-7 from the supernatant using a higher RPM by centrifugation. The crystals so synthesized, using Zn:HbIm molar ratios of 1:4 and 1:8, are labelled as ZIF-7(14)-L, ZIF-7(14)-S, ZIF-7(18)-L and ZIF-7(18)-S, where "L" and "S" suffixes represent larger and smaller particle sizes. This enables us to understand the adsorption behaviour of flexible MOFs with a relatively narrow size distribution for the first time.

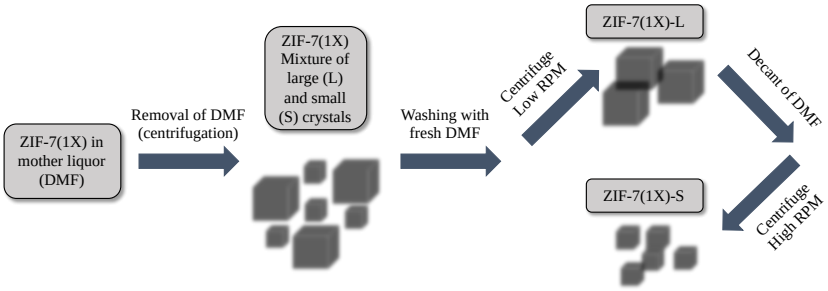

Figure 2: Schematic of 2-step separation to isolate larger-sized (L, μm) and smaller-sized (S, nm) crystals from the same batch of synthesis.

Stirring (STR)

The solvothermal synthesis was modified by stirring as represented in Fig. 1. This strategy was used to obtain better uniformity and smaller crystal size. Unlike the previous methods, the synthesis mixture was continuously stirred at 373 K in a closed Schott bottle for 24 hours. As before, we used the three different Zn:HbIm molar ratio of 1:2, 1:4 and 1:8 to modulate the crystal size. After stirring at 373 K for 24 h, the solid was separated, washed, and dried. These three batches are labelled as ZIF-7(12)-STR, ZIF-7(14)-STR and ZIF-7(18)-STR, respectively.

Zinc acetate dihydrate as precursor

We also synthesized ZIF-7 as reported by Tu *et al.*[50], where at first, solution of 10 mmol (2.19 g) of $Zn(CH_3COO)_2.2H_2O$ in 100 mL of DMF and 20 mmol (2.36 g) of HbIm in 100 mL of methanol were prepared. The Zn-acetate solution was added to the ligand solution under stirring at room temperature. The mixture immediately turned thick white and was stirred for 1 h. After that, the solid was separated and washed with methanol and dried at 353 K overnight. The sample was labelled as ZIF-7(OAc) hereafter.

CHARACTERIZATION TECHNIQUES

Ex situ PXRD measurements were performed on a Stoe Stadi P diffractometer in transmission geometry using monochromatic $CuK_{\alpha 1}$ radiation (λ= 0.154056 nm) and

MYTHEN detector (DECTRIS) with the step scan with 6° steps and the exposure time of 120 seconds per step.

Particle size distribution and morphology of the synthesized materials were analysed using Hitachi S-4800 and SU-8000 scanning electron microscope (SEM). ImageJ (version 1.53) software was used for SEM image analysis. We have described larger crystals of size > 0.5 μm as micron-size and crystals in the range 0.5 – 0.05 μm as meso-size. We also calculated the polydispersity index (PDI, defined as the square of the ratio of standard deviation to the mean) to evaluate the heterogeneity of the synthesized ZIF-7.

Thermogravimetric – differential thermal analysis (TG-DTA) was carried out from 30° to 800°C, with a heating rate of 5 K/min, in NETZSCH STA 409C/CD under a continuous flow of synthetic air.

BELSORP-max (Microtrac MRB) volumetric low-pressure adsorption device was used for measuring isotherms of gases and vapours. Prior to the adsorption measurements, the materials were activated at 453 K and 10^{-3} mbar dynamic vacuum overnight in a Schlenk line to remove solvent molecules from its pore.

In situ PXRD was performed on ZIF-7 while undergoing adsorption and desorption of CO_2 at 195 K and 298 K using a customized setup, based on laboratory powder X-ray diffractometer Empyrean-2 (PANALYTICAL GmbH), equipped with closed-cycle helium cryostat (ARS DE-102) and home-built *in situ* cell, connected to volumetric adsorption instrument BELSORP-max (Microtrac MRB). The TTL trigger was used for establishing the communication between BELSORP-max and Empyrean software and to ensure the data collection of the adsorption isotherm and PXRD pattern in a fully automated mode at the pre-defined points of the isotherm. The parallel Cu Kα1 beam was generated for the data collection using W/Si mirror and hybrid 2xGe(220) monochromator, 4 mm mask, and primary divergence and secondary anti-scatter slits with 1/4° opening. A Pixcel-3D detector in 1D scanning mode (255 active channels) was

used for measuring reflection intensities. The diffraction experiments were performed using ω–2θ scans in transmission geometry in the range of 2θ = 5-50°.

PXRD patterns containing earlier reported phases ZIF-7-I (OP) and ZIF-7-II (CP) were analysed using Le Bail profile fit, implemented in the FullProf software.[51] PXRD patterns, measured at high CO_2 loadings at 195K have been indexed using DICVOL04[52] and obtained monoclinic unit cell was further refined using Le Bail profile fit.

RESULTS AND DISCUSSIONS

The as-synthesized ZIF-7 has an open pore (OP) framework, also known as ZIF-7-I. The phase purity of all samples was confirmed by PXRD showing good matching with the ZIF-7-I form reported by Zhao *et al.*[29,53] (ESI, Fig. S1a and S1b). The phase transition of ZIF-7 can be observed upon desolvation: Fig. 3 demonstrates the contraction of ZIF-7 crystal structure, leading to the formation of the close pore (CP) phase known as ZIF-7-II. We observed that ZIF-7-II state is retained under atmospheric conditions at least up to 3 months based on the PXRD profile (Fig. S2). Reopening from ZIF-7-II to ZIF-7-I is possible by stirring the activated powder in DMF overnight (Fig. S2). Several other guest molecules, including CO_2 can induce this phase transition process, which is thoroughly explored in our work under *in situ* experimental conditions.

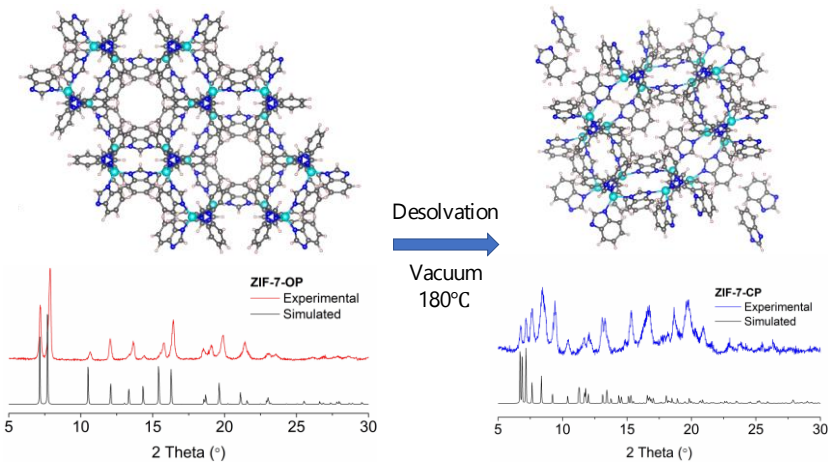

Figure 3: Phase transition of ZIF-7 (C = grey, N = blue, H = off-white, Zn = cyan) before and after desolvation (CIF file by Zhao et al.[53])

Textural properties

We varied the molar concentration of HbIm ligand in static solvothermal (without stirring) synthesis and dynamic synthesis with stirring to control the nucleation and crystal growth in MOF samples (Fig. 1 and 2). As will be reported later, stirring results in more uniform sub-micron sized crystals and affects particle agglomeration as well. To understand the influence of the metal salt on the resulting product, stirring synthesis was repeated with zinc acetate. The effect of linker concentration and alternate zinc sources on particle downsizing is reported for ZIF-8,[54,55] motivating us to employ a similar concept for crystal size variation.

The PXRD of all samples show a good match with the ZIF-7-I structure (ESI, Fig. S1a and S1b). TG-DTA for the as-made materials (Fig S4) are indistinguishable, where the final weight for all the samples was ~24%, highlighting similar composition despite changes in the synthesis procedure. Hence, we can eliminate the probability of impurity within the framework.

The textural properties for all as-synthesized ZIF-7 samples, analysed using SEM and N_2 adsorption measurements at 77 K are discussed in the following subsections. The size distribution is described using polydispersity index, PDI = (standard deviation/mean)^2. Detailed SEM images of all the materials can be found in Fig. S3.

Solvothermally Synthesized ZIF-7

The solvothermal synthesis resulted in micron-size particles, in the range of 15 – 4 μm, with broader size distribution, as shown in Fig. 4. As we increased HbIm concentration, the crystal size decreased in the order ZIF-7(12) > ZIF-7(14) > ZIF-7(18). All these samples crystallized in rhombic dodecahedron morphology, with ZIF-7(12) and ZIF-7(14) showing the best crystallinity (detailed images: ESI, Fig. S3(a)). On the other hand, ZIF-7(18) showed a broader

particle size distribution. Note that the size distribution broadened further when the synthesis temperature was reduced to 373 K (ZIF-7(18)-373, reported in ESI Fig S3(a)). The images also revealed existence of small, agglomerated crystals, predominantly in ZIF-7(18). The presence of this smaller crystals (< 0.5 μm) impacts N_2 and CO_2 adsorption.

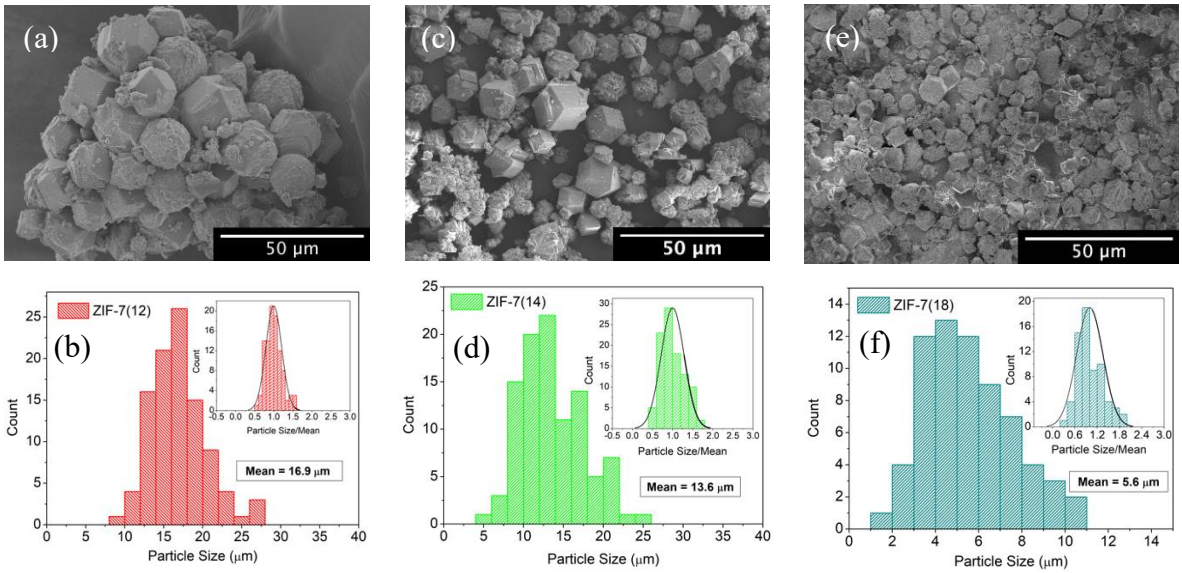

Figure 4: SEM images and size distribution of solvothermally synthesized ZIF-7s: [a,b] ZIF-7(12); [c,d] ZIF-7(14); and [e,f] ZIF-7(18). The insets show the normalized size distribution.

An initial assumption based on the kinetic diameter suggests that N_2 molecule (0.36 nm) may not be able to enter in ZIF-7 pores (window diameter: 0.3 nm).[56] Fig. 5 shows that depending on the crystallite size, the framework adsorbs different amounts of N_2 at 77 K showing a narrow hysteresis between adsorption and desorption curves in most cases. Caudrado-Collados *et al.*[57] also reported a similar type of N_2 adsorption isotherms on nano-ZIF-7 and thoroughly investigated the importance of solvent exchange for accessing the narrow pores. However, we showed that DMF did not impose a problem and can be removed from the narrow pores at elevated temperature under vacuum (Fig. S2) resulting in similar type of isotherms. Fig. 5(a) shows an increase in N_2 uptake as the mean particle size is reduced from 15 μm to 5 μm, though the effect of broader crystal size distribution becomes unavoidable.

We attempted to modify the crystal size by repeating ZIF-7 synthesis at a lower temperature. The results presented in ESI Fig. S5 for ZIF-7(18)-373 (i.e., ZIF-7(18) solvothermal synthesis at 100 °C) indicate that, in spite of a similar mean size ~4 μm, the presence of higher number of smaller crystals in ZIF-7(18)-373 compared to ZIF-7(18) seems to be responsible for their significant N_2 uptake.

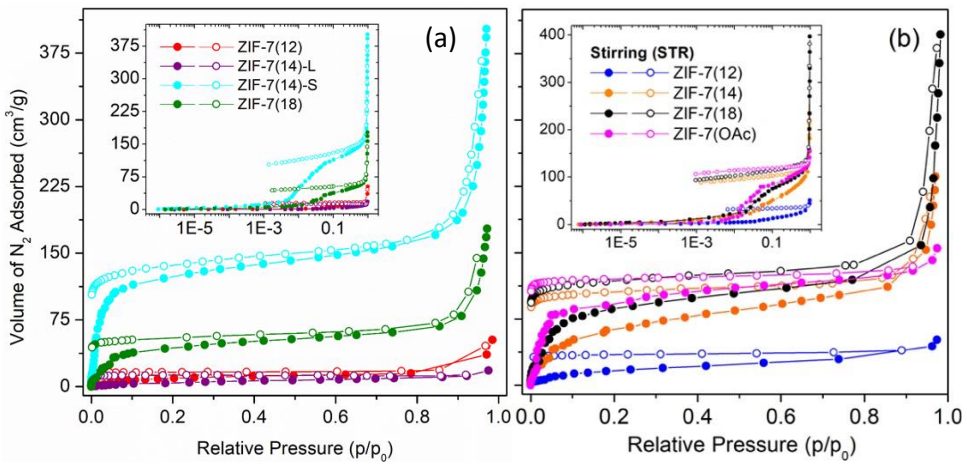

Figure 5: N_2 adsorption isotherms at 77 K of ZIF-7 samples synthesized using (a) solvothermal and (b) stirring conditions.

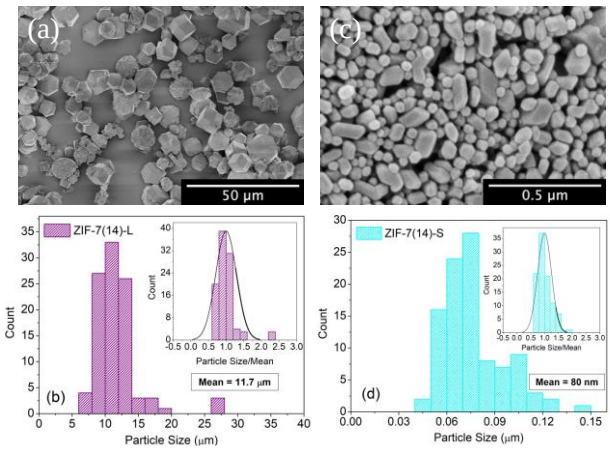

Figure 6: SEM images and size distribution of [a,b] ZIF-7(14)-L; and [c,d] ZIF-7(14)-S

Since solvothermal synthesis does not provide precise control over particle size distribution, we repeated the synthesis using two-step centrifugation for separating micron-sized (ZIF-

7(14)-L) and nano-sized (ZIF-7(14)-S) crystals from the same batch. Fig. 6 shows the SEM images and the corresponding size distribution for ZIF-7(14)-L (11.7±3.43 μm) and ZIF-7(14)-S (0.08±0.02 μm). The nano-ZIF-7(14)-S with a mean crystal size of 0.08 μm has an increased N_2 uptake, implying the CP – OP transition.[57] The non-overlapping desorption branches (insets in Fig. 5) is indicative of retention of the OP phase at 77 K with N_2 up to 10^{-3} p/p_0. These inferences are supported by the expansion in experimental pore volume calculated at 0.8 p/p_0 in Table 1. In summary, the effect of a broad size-distribution on adsorption is discussed for the first time. Micron-size crystals seem to be incapable of CP – OP transition on N_2 adsorption at 77 K, whereas a significant N_2 adsorption could indicate presence of < 0.5 μm size crystals.

Table 1: Textural properties of various ZIF-7 samples

Name	Size with Std. Dev (μm)	Poly Dispersity Index (PDI)	N_2 Pore Volume at 77 K & 0.8 p/p_0 (cm^3/g)
ZIF-7(12)	16.9±3.51	0.043	0.02
ZIF-7(18)	5.6±1.99	0.126	0.09
ZIF-7(14)-L	11.7±3.43	0.086	0.01
ZIF-7(14)-S	0.08±0.02	0.062	0.24
ZIF-7(12)-STR	0.42±0.19	0.2	0.05
ZIF-7(14)-STR	0.18±0.09	0.246	0.16
ZIF-7(18)-STR	0.06±0.02	0.073	0.18
ZIF-7(OAc)	0.14±0.03	0.044	0.18

ZIF-7 Synthesized using Stirring (STR) method

The stirring method led to a reduction in crystal size and narrowing the crystal size distribution for the same metal/ligand ratio compared to solvothermal synthesis. The crystal sizes decreased with increase in the HbIm concentration. In contrast, ZIF-7(OAc) crystallized in spherical morphology with a similar ~0.15 μm average size. The sizes of the stirred ZIF-7 as well as their distribution are shown in Fig. 7.

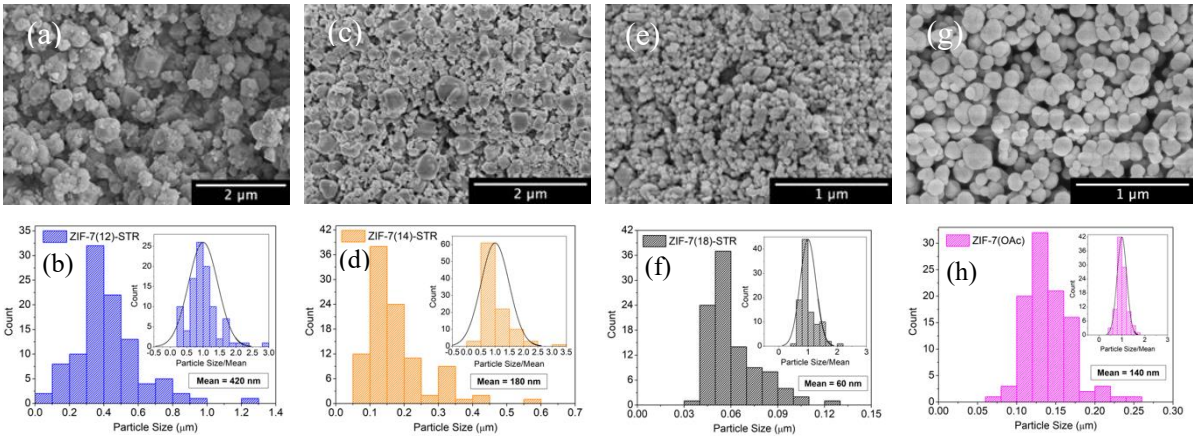

Figure 7: SEM images and size distribution of 'STR' ZIF-7 samples: [a,b] ZIF-7(12)-STR; [c,d] ZIF-7(14)-STR; [e,f] ZIF-7(18)-STR; and [g,h] ZIF-7(OAc)

The N_2 adsorption isotherms in Fig. 5(b) show similar behaviour for ZIF-7(14)-STR and ZIF-7(18)-STR and ZIF-7(OAc), aligned with previous inference (*c.f.* Caudrado-Collados *et al.*[57]) of a critical crystal size of < 0.5 µm for CP–OP transition with N_2 at 77 K. However, despite their crystal size of 0.42±0.19 µm, ZIF-7(12)-STR samples showed an unexpected behaviour, which cannot be explained only based on the crystal size variation. Specifically, N_2 adsorption of ZIF-7(12)-STR is qualitatively similar to ZIF-7(12) despite significant difference in their size (Fig. 5 and Table 1). This ambiguity could have originated from the difference in the morphology or defect formation[58–60] because of rapid nucleation and crystal growth in stirring synthesis conditions. Fig. S6 in the ESI compares N_2 adsorption isotherms for a few of the samples, showing that the distribution of crystal size is also relevant, perhaps indicating that the presence of a significant percentage of meso-size crystals of < 0.5 µm size may be necessary for the phase transition with N_2 to take place. Although most of the analysis presented here and summarized in Table 1 indicates a critical size of ZIF-7 to be < 0.5 µm for the CP to OP transition, the N_2 uptake of ZIF-7(12)-STR does not support this generalization.

Insights into new CO_2 filled open phase of ZIF-7 by *in situ* PXRD

Adsorption of carbon dioxide on ZIF-7 framework at 298 K was first reported by Aguado *et al.*[20] with an S-type isotherm and a hysteresis. Such behaviour is interesting for CO_2 capture application. Since the gate-opening behaviour of ZIF-7 is sensitive to the adsorbate molecule, several authors have investigated ZIF-7 framework switchability using N_2, Ar, CO_2, CH_4.[30,31,61] This motivated us to investigate the structural evolution of ZIF-7 in parallel with adsorption of guest molecules. We first investigate gate-opening behaviour with CO_2 at low temperature, followed by the effect of particle size and morphology CO_2 adsorption at near-ambient conditions, and finally vapor adsorption.

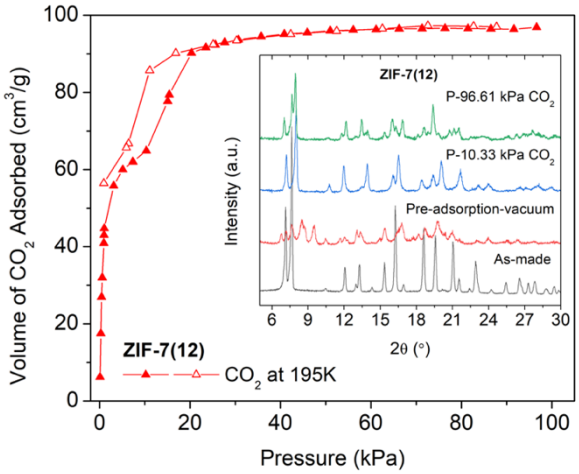

Figure 8: *In situ* PXRD (inset) in parallel with CO_2 adsorption at 195 K on ZIF-7(12)

Fig. 8 shows the CO_2 adsorption at 195 K in parallel with *in situ* PXRD. At 195 K, all the ZIF-7 samples showed qualitatively identical behaviour (see ESI, Figs. S10, S12, S14, S16, S18 and S20). Here, we elaborate the result of ZIF-7(12) alone. The CO_2 uptake capacity at 195 K was 96 $cm^3(STP)g^{-1}$ at $p/p_0 = 0.8$ (which is double the capacity compared to the isotherm at 298 K). In Fig. 8, the first step corresponds to the transition ZIF-7-II (CP) → ZIF-7-I (OP1), earlier reported by Zhao et. al.[29] The second step, however, corresponds to the yet unknown transition from ZIF-7-I (OP1) to ZIF-7-I (OP2). Although this two-step transition was reported earlier,[62] there is still a lack of structural information related to this transition. These changes

involve splitting and shifting of reflections presumably suggesting an expansion of ZIF-7 pores with an additional arrangement of CO_2 molecules.

The PXRD pattern corresponding to the first step of the CO_2 isotherm in Fig. 8 exhibited a slight shift in the peak positions (blue line in Fig. 8 inset) compared to the as-synthesized ZIF-7 with DMF filling the pores (black line) in the range of $2\theta = 5\text{-}25°$. Le Bail fit of PXRD profile indicated that the unit cell of as-synthesized ZIF-7 is ~400 $Å^3$ larger compared to CO_2 filled phase at 195 K and 5 kPa (Table 2). As this indicates a partially opened ZIF-7, we studied the phase transition thoroughly under CO_2 adsorption at 195 K. The indexing of PXRD pattern of OP2 phase resulted in the monoclinic unit cell (*C*2/*m* space group) with an acceptable fit of all observed reflections. The analysis of group-subgroup relations suggests direct relation between $R\bar{3}m$ and *C*2/*m* with an index of 3. The structural model (Table S3, ESI), simulated in Materials Studio 5.0 using UFF-force field, and containing four CO_2 molecules per asymmetric unit, shows a quite good match with experimental data (Fig. S26, ESI). However, the quality of PXRD data does not allow to conduct Rietveld refinement. The unit cell parameters for selected PXRDs, measured at specific gas pressure and temperature conditions are provided in Table 2. After reducing the symmetry of OP1 phase from $R\bar{3}m$ to *C*2/*m* space group, the unit cells of OP1 and OP2 can be directly compared. Increasing of the *a* and *b* axes with simultaneous decreasing of *c* axis and reducing of monoclinic angle (Table 2) leads to increase in the unit cell volume by 185 $Å^3$, which proves the higher porosity of OP2 phase. Analyses of *in situ* PXRD patterns indicate a high cooperativity of the phase transitions showing the co-existence of OP1 and OP2 phases in the narrow pressure range. The unit cell volumes, normalized per Zn atom remain constant within the existence range of defined phase (ESI, Fig. S25). The evidence from the unit cell parameter also suggests swelling of the ZIF-7 framework in the $R\bar{3}m$ space group as we notice expansion of the cell volume by elongation along *a* and *b* axes for CO_2, MeOH and DMF as respective guest species.

Table 2. Unit cell parameters, refined for ZIF-7(12) under different gas pressure and temperature conditions except for MeOH adsorption.

Conditions	Phase	Space group	*a* (Å)	*b* (Å)	*c* (Å)	α (°)	β (°)	γ (°)	V (Å^3)
DMF, 298 K	as made	$R\bar{3}m$	23.0824(4)	23.0824(4)	15.7049(4)	90	90	120	7246.5(3)
Vacuum, 298 K	CP	$P\bar{1}$	23.716(3)	21.466(3)	16.118(2)	91.39(1)	91.96(1)	108.63(1)	7766(2)
CO_2 100 kPa, 298 K	OP1	$R\bar{3}m$	22.483(1)	22.483(1)	15.833(1)	90	90	120	6930.7(6)
Vacuum, 195 K	CP	$P\bar{1}$	23.647(2)	21.469(2)	16.189(2)	90.88(1)	92.18(1)	108.98(1)	7763.3(14)
CO_2 5 kPa, 195 K	OP1	$R\bar{3}m$	22.048(1)	22.048(1)	16.004(1)	90	90	120	6737.6(6)
CO_2 5 kPa, 195 K	OP1	*C2/m*	16.609(1)	22.048(1)	16.003(1)	90	129.97(1)	90	4491.2(6)
CO_2 100 kPa, 195 K	OP2	*C2/m*	17.155(1)	23.040(1)	13.486(1)	90	118.665(5)	90	4676.8(4)
ZIF-7(OAc), MeOH 13 kPa, 298 K	OP1	$R\bar{3}m$	22.8848(7)	22.8848(7)	15.5771(7)	90	90	120	7064.9(5)

In terms of the unit cell volume, all three crystal structures show comparable values (Table 2). Interestingly, ZIF-7 CP structure shows even higher unit cell volume (7766 Å^3) compared to ZIF-7 OP structure (6737.6 Å^3) although both contain 18 Zn atoms per unit cell. It indicates that, not the unit cell volume alone, but rather accessibility of the pores and in particular pore windows are of paramount importance for guest-induced flexibility. This has been also pointed out for ZIF-8.[63] The calculations of the probe-accessible volume for all three structures using Zeo++ software[64] for the probe molecule with kinetic diameter of carbon dioxide (3.3 Å) indicate that ZIF-7 CP and ZIF-7 OP1 contain only non-accessible probe-accessible volume, whereas in ZIF-7 OP2 the larger part of pore volume is accessible for CO_2 (Table 3).

Table 3. Geometric calculations of probe-occupiable volume for CO_2.

Structural model	Accessible probe-occupiable volume (cm^{3}g^{-1})	Non-accessible probe-occupiable volume (cm^{3}g^{-1})
ZIF-7 CP	0	0.169
ZIF-7 OP1	0	0.204
ZIF-7 OP2	0.183	0.067

CO_2 Adsorption at 298 K in ZIF-7

In contrast to nitrogen physisorption, all ZIF-7 samples of 15 – 0.05 μm range undergo CP to OP transition showing a pronounced hysteresis in CO_2 physisorption isotherms at 298 K. As described by Coudert *et al.,* the stepped isotherm is a result of the difference in the free energy between the OP and CP phase ($F_{op} < F_{cp}$) when OP phase can be stabilized by the guest.[65] Furthermore, the activation barrier for the CP – OP transition can be crossed owing to the overpressure Δp ($\Delta p = p_g - p_e$: where p_g is gating pressure and p_e is equilibrium pressure and $p_g > p_e$) leading to stabilization of the OP phase with guest molecule by lowering the free energy change.[66,67] However, since all materials show a transition with CO_2, the corresponding isotherms were analyzed in details.

Solvothermally Synthesized ZIF-7 materials

CO_2 adsorption behaviour and the first derivative of adsorption and desorption branch are shown in Fig 9(a), (b) and (c) respectively. All the materials including ZIF-7(14)-S nanocrystals, show gate-opening behaviour. The gate-opening and closing pressure remains constant and does not show any crystal size dependency for the micro-size crystals. However, the presence of meso-size crystals in ZIF-7(18) results in a second inflection point beyond the pressure at half maximum uptake. This behaviour is likely an effect of the broader crystal size distribution in the same batch of materials.

The effect of size distribution is corroborated by analysing the CO_2 adsorption of samples separated by two-step centrifugation, with the larger and smaller sized samples with L and S suffixes. In Fig. 9 the isotherm of ZIF-7(14)-S crystals with an average size of 0.08 μm, possesses a delayed gate-opening owing to two orders of magnitude reduction in crystal size. A detailed discussion is presented in the supporting information (ESI, Figs. S7, S8; Table S2) on the effect of crystal size distribution. Specially, Figs S7 and S8 indicate that the two peaks in the conventional solvothermal ZIF-7s approximately corresponding to the individual peaks in the "L" and "S" samples.

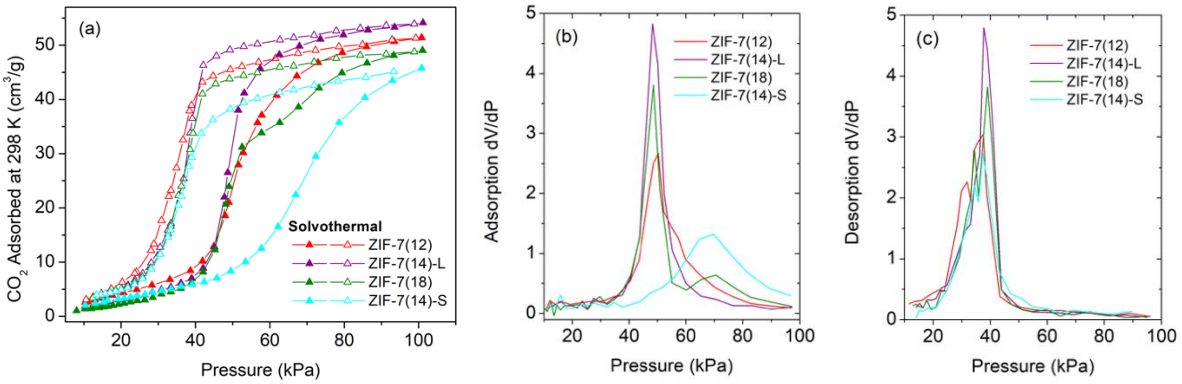

Figure 9: (a) CO_2 adsorption isotherms at 298 K for solvothermally synthesised ZIF-7; and first derivatives of the respective (b) adsorption and (c) desorption branches.

The gate-opening pressure is doubled for ZIF-7(14)-S due to size reduction. However, the closing pressure remains same for all the solvothermally synthesized ZIF-7 irrespective of size, exhibited by the derivative plots in Fig. 9(b) and (c). These plots qualitatively describe the trend of activation energy barrier of the phase transition in flexible frameworks.[45] The steepness of the adsorption branch is relatable to the narrow distribution of free energy of activation. Whereas with the presence of meso-size crystals, the adsorption branch exhibited two distinct peaks, approximately at 45 kPa and 65 kPa (ZIF-7(18)), representing different free energies of activation for CP to OP transition for micron and meso-size crystals in the samples.

ZIF-7 Synthesized using Stirring

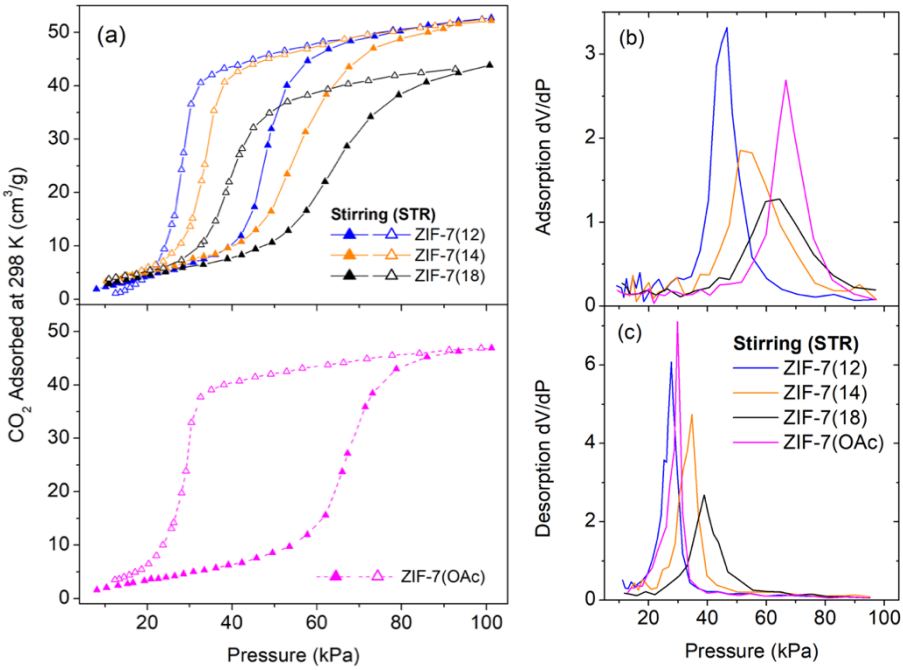

Figure 10: (a) CO_2 adsorption isotherms at 298 K for various ZIF-7 synthesized under stirring; and the first derivatives of the respective (b) adsorption and (c) desorption branches.

Fig. 10 shows the CO_2 adsorption isotherms and the respective first derivatives. Despite their nano-sized crystals, all the materials show S-shape isotherms albeit with broad hysteresis. Interestingly, with decrease in crystal size both gate-opening and closing pressure changed systematically unlike other flexible MOFs.[45,68] This observation either indicates that both, opening and closing, are far from equilibrium or the equilibrium transition pressure is affected by factors other than size, such as morphology or defects. To provide evidence for this hypothesis advanced experimental or simulation tools are required and are beyond the scope of this work. The CO_2 uptake capacities and respective CP to OP transition pressure and vice-versa at the half maximum uptake is noted in table 4. Despite an average size of 0.42 μm, ZIF-7(12)-STR behaves identically to ZIF-7(12) disturbing a simple trend of assuming a critical size for both N_2 and CO_2 adsorption.

The CO_2 adsorption isotherm of ZIF-7(OAc), which crystallizes in spherical morphology with an average size of 0.15 μm possesses the widest hysteresis with gate-opening and closing

pressure around 65 kPa and 29 kPa. This underlines the effect of crystal morphology on guest-induced framework flexibility, previously reported for MIL-53(Al) and NH_2-MIL-53(Al)[69,70] is applicable for ZIF-7 nano-crystals. Conversely, ZIF-7(14)-L showed the narrowest hysteresis (see ESI, Fig. S8) among all samples analyzed.

Table 4: CO_2 adsorption data at 298 K

Materials		CO_2 Uptake at 100 kPa (wt %)	CP-OP & OP-CP Transition Pressure (kPa)	Materials		CO_2 Uptake at 100 kPa (wt %)	CP-OP & OP-CP Transition Pressure (kPa)
Solvothermal	ZIF-7(12)	10.1	50 & 34	Stirring	ZIF-7(12)-STR	10.3	46 & 27
	ZIF-7(18)	9.6	50 & 36		ZIF-7(14)-STR	10.3	55 & 34
	ZIF-7(14)-L	10.6	49 & 37		ZIF-7(18)-STR	8.6	62 & 39
	ZIF-7(14)-S	9.0	67 & 37		ZIF-7(OAc)	9.2	65 & 29

CO_2 induced structural evolution by *in situ* PXRD

The mechanism of CO_2 induced phase transition of ZIF-7 demonstrated by Zhao *et al.,* initiates by accumulation of CO_2 in the distorted hexagonal 6-ring window followed by rotation of the shared bIm linker between normal and distorted 6-ring through CO_2 migration; resulting in the abrupt increase of gas uptake.[29] This points out the possibility of the apparent diffusivity being affected by increasing surface resistance rather than intracrystalline mass transfer resistance similar to ZIF-8.[68] This has intrigued us to ask the question: 'What determines the delay in CP to OP transition in ZIF-7? Is it the surface barrier or intra-crystalline diffusion?' The *in situ* PXRD experiments conducted in parallel to CO_2 adsorption shown in Fig. 11, indicated shift in the pressure from 45 kPa for ZIF-7(12) to 55 kPa for ZIF-7(18)-STR, where the PXRD of CP phase starts to evolve towards OP phase. This is indicative of ZIF-7 existing in the CP phase until 55 kPa CO_2 pressure for ZIF-7(18)-STR having average crystal size < 0.1 μm, whereas the pressure is 45 kPa for ZIF-7(12) possessing crystals > 10 μm. This concludes that the delay in gate-opening for ZIF-7 is due to increase in the surface barrier, as the nucleation for gating transition initiates at the outer surface of the crystals. The two orders of

magnitude reduction in crystal size of ZIF-7(18)-STR in comparison to ZIF-7(12), results in higher surface to volume ratio with a greater number of weaker surface adsorption sites causing a delay for the phase transition. This insight was motivated by the molecular simulation by Zhang *et al.* on ZIF-8, showing that the weaker affinity of surface adsorption sites due to lack of neighbouring groups[41] increases the activation energy barrier to initiate gate-opening, require larger adsorbate concentration to trigger dynamic behaviour.[71–73]

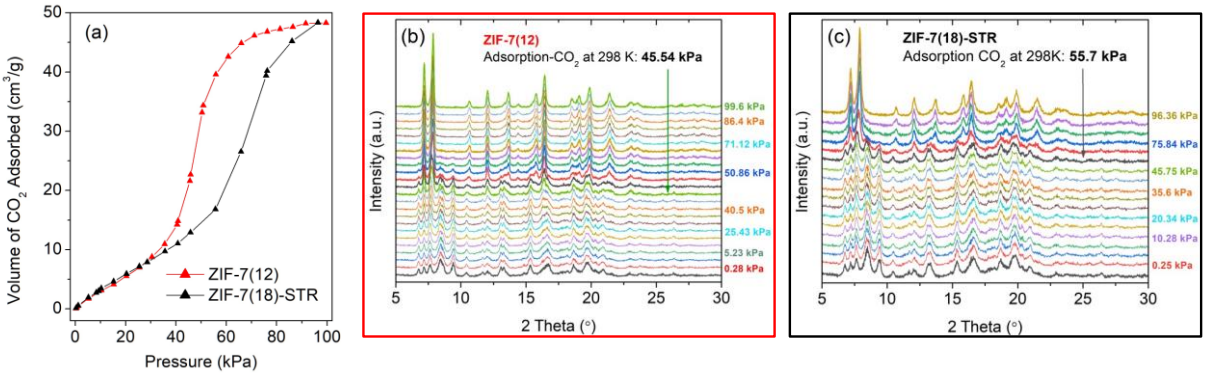

Figure 11: *In situ* PXRD in parallel to CO_2 adsorption at 298 K for ZIF-7(12) and ZIF-7(18)-STR (a) adsorption isotherms; structural evolution during adsorption (b) ZIF-7(12) and (c) ZIF-7(18)-STR

We have investigated the CO_2 adsorption on ZIF-7(12), ZIF-7(18), ZIF-7(12)-STR, ZIF-7(18)-STR and ZIF-7(OAc) under *in situ* PXRD conditions (ESI, Figs. S11 – S20). Studying multiple samples confirmed that their intrinsic phase transition behaviour does not change except for the pressure to trigger the transition. The CO_2 adsorption isotherms described before for 'STR' samples exhibit unique features as both gate-opening and closing pressure systematically changes, which cannot be explained by crystal size alone. It will require further studies on identifying possible reasons such as defects on the surface or in bulk structure, agglomerations, or the morphology to understand this phenomenon, which is beyond the scope of this study.

Summarizing, *in situ* PXRD provide the understanding guest-induced transitions in ZIF-7 samples under controlled CO_2 loadings at both 298 K and 195 K. However, the comparison of

CO_2-filled phases with DMF filled framework indicates that the latter shows the most expanded form, which we named it as $OP1^+$ from here on. Also, despite the limitations of smaller pore aperture, ZIF-7 is capable of adsorbing much larger molecules than its pore opening, highlighting the significance of host-guest interactions. Thus we analysed vapour adsorption isotherms using alcohols possessing significant dipole moment to interact strongly through H-bonding[29], or heptane and toluene showcasing hydrophobic or π-π interaction, rendering CP – OP transition in ZIF-7 as well as CO_2 or N_2 which are non-polar in nature. This leads us to the following section on solvent vapour adsorption.

Solvent vapour adsorption on ZIF-7

ZIF-7(12) and ZIF-7(18)-STR were studied for sorption of alcohols and organic solvents to compare the effect of crystal size. The isotherms shown in Fig. 12 suggest that irrespective of small pore window of ZIF-7, larger guests can enter the pores inducing CP to OP transition. Among methanol, ethanol, and iso-propanol the latter two exhibited type-I isotherms whereas methanol exhibits hysteresis, implying weaker interaction with ZIF-7. However, the crystal size does not affect the gate-opening pressure, which is presumptively by lowering the activation energy barrier due to the stronger H-bonding type interactions. Furthermore, alcohol adsorption isotherms in Fig. 12 do not attain a plateau implying adsorption at inter-particle pores or swelling of ZIF-7 framework. A simple calculation of pore volume reported in table S2, supports the idea of framework swelling. The table shows that with increase in the alcohol size the calculated pore volume increases suggesting expansion of framework. This volume is further increased for nano-crystals possessing interparticle pores.

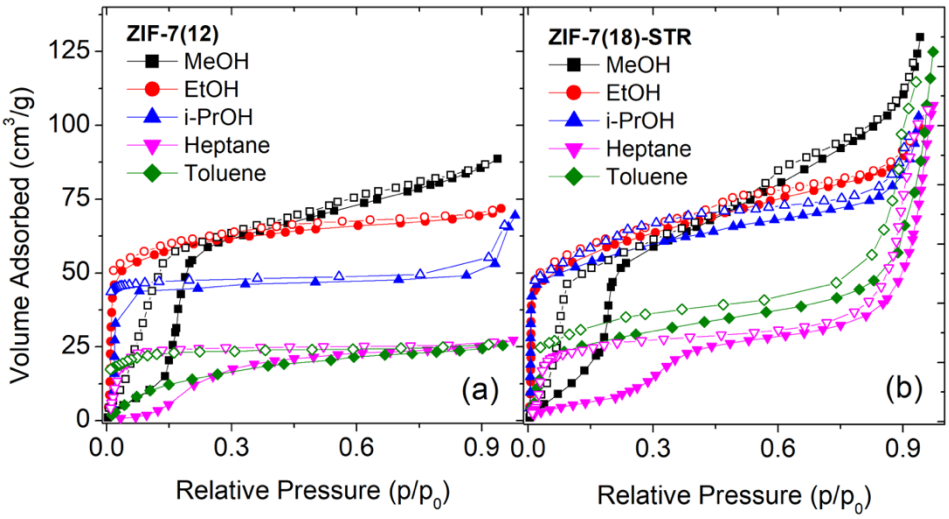

Figure 12: Solvent vapours physisorption at 298 K on (a) micron size crystals: ZIF-7(12), (b) sub-micron crystals: ZIF-7(18)-STR

Furthermore, we show adsorption of heptane and toluene for the first time, revealing a prominent π-π stacking interaction between toluene and HbIm of ZIF-7 framework resulting in steeper uptake at lower relative pressure whereas heptane shows hysteresis around $p/p_0 = 0.2 – 0.3$. Also, it can be seen for meso-size crystals of ZIF-7(18)-STR that the gate-opening by heptane is at higher relative pressure than for micron size crystals of ZIF-7(12).

Considering differences in host-guest interactions, there is a window for ZIF-7 to be investigated for n-heptane/toluene[74] and alcohol/water separation[75], as these are of significantly important industrial processes. Hydrophobicity of ZIF-7 was tested by H_2O vapour adsorption (ESI Fig. S9). Since ZIF-7 exhibits a favourable uptake of ethanol and IPA at low relative pressure, while water uptake is unfavourable until 0.8 relative pressure, could be valuable for water/alcohol separation. On the other hand, ZIF-7(18)-STR shows a prominent type-I isotherm for toluene, whereas *n*-heptane isotherm shows a hysteresis loop, implying possibility for their separation.

In situ PXRD in parallel to MeOH adsorption

The presence of extra-large pores like the as-made ZIF-7 was observed through the *in situ* PXRD experiment carried out in parallel with MeOH adsorption at 298 K. Du *et al.* have investigated the expansion of ZIF-7 while adsorption of C1-C5 alcohols, where with increase in the alcoholic carbon chain the XRD peaks shift to lower angles.[32] We used ZIF-7(OAc) considering the uniformity and presence of discreet particles to avoid condensation in interparticle pores and to obtain data relatable to the framework porosity. In Fig. 13 we observe the gradual change from CP to OP phase during MeOH adsorption. A comparison of PXRD peaks of CO_2 with DMF, or MeOH molecules in ZIF-7 pores suggested that the difference in XRD peaks probably arose due to different arrangement of adsorbate species inside the pores. Solvents such as DMF and MeOH interact more strongly with framework, opening it into an extra-large pore configuration in comparison to CO_2 (Table 2). The extra-large opening of ZIF-7 in presence of solvents is named as $OP1^+$. Profile fit of PXRD patterns indicates the direct reversible transition between CP to $OP1^+$ phases (ESI, Figs. S22 & S23) showing pronounced inelastic deformations of the unit cell upon adsorption and desorption of the fluid.

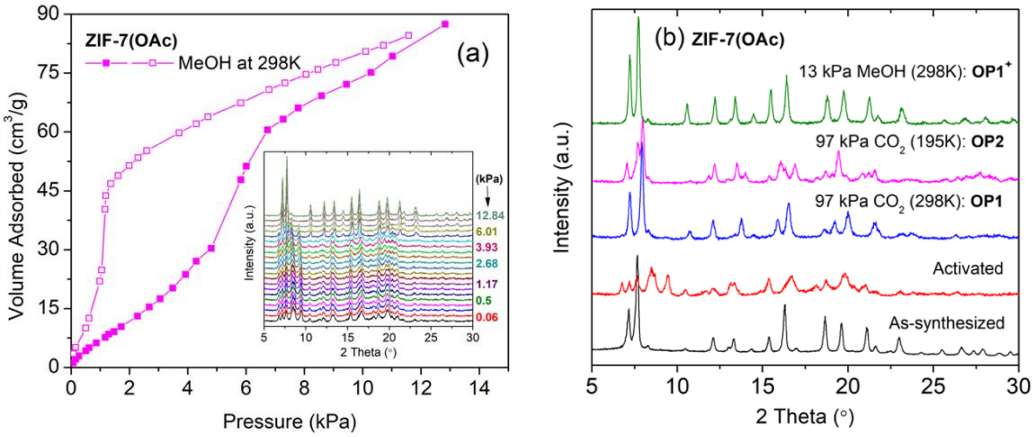

Figure 13: (a) *In situ* PXRD measurement in parallel to MeOH physisorption on ZIF-7(OAc) at 298 K and (b) comparison of XRD with different guest molecules in the pores

CONCLUSIONS

ZIF-7 is a flexible MOF that shows gate-opening behaviour in presence of CO_2 as guest molecule under near ambient conditions. We showed that ZIF-7 framework synthesized using

different methodologies affect the guest-responsive properties of the solid. The effect of crystal size and its distribution on both N_2 and CO_2 adsorption behaviour was analysed. Static solvothermal method produces crystals with defined morphology and mean size ranging between 4 to 17 μm depending on ligand concentration in precursor solution with a rather broad size distribution. The stirring method, in contrast, results in smaller (0.05 – 0.5 μm) sized crystals with undefined polyhedral morphology and agglomeration.

ZIF-7 was known to exhibit CP → OP transition in response to guest molecules. For the first time, we report a yet unknown CO_2-filled ZIF-7 phase (OP2) at 195 K showing larger pore opening and adsorption capacity than the OP1 phase. Using *in situ* PXRD measurement in parallel to CO_2 and MeOH adsorption we compared the various guest filled ZIF-7 phases abbreviated as OP1, OP2 and $OP1^+$. With solvent molecules inside ZIF-7 pores, the framework swelled to $OP1^+$ phase. Thus host-guest interaction plays a pivotal role for complete opening of the ZIF-7 framework.

Unlike many other flexible MOFs, ZIF-7 remains flexible upon CO_2 adsorption at ambient conditions even with a crystal size of < 0.1 μm, which is useful for various gas separation applications. The difference in the "gate opening" pressure upon adsorption of CO_2 at 298 K is rather small, varying between 35 and 65 kPa with different slopes depending on the crystal size, their distribution and morphology. Furthermore, the *in situ* PXRD suggested that the delay in the gating pressure for CO_2 is due to the enhanced surface barrier as the peaks remain at CP phase until the inflection point in CO_2 adsorption isotherm at 298 K.

The solvothermally synthesized ZIF-7 did not show any change in "gate closing" pressure during desorption, as previously reported for other MOFs. In contrast, stirring synthesis resulted in smaller ZIF-7 crystals, which not only showed flexibility in nano-sized crystals but also size-dependent "gate closing" pressures. This unique adsorption behaviour of 'STR' ZIF-7 samples, where both "gate opening" and "gate closing" pressure changes, can also originate

from surface defects such as grain boundaries and intercrystalline strains. The understanding of these effects is still in its infancy and remains as an open question in MOF research. This work also revealed the possibility of reducing the hysteresis width between adsorption and desorption curves using larger size particles with narrow size distribution. Our findings can be useful for development of industrially viable standard synthesis protocols of ZIF-7 for application in sustainable gas separation processes. Further investigation of these effects by advanced experimental and simulation tools could enlighten the thermodynamics and kinetic barriers of this system.

ASSOCIATED CONTENTS

The supporting information is available as PDF file. It contains detail of *in situ* PXRD, Le Bail refinement and Zeo^{++} calculations. We have also reported material characterizations such as PXRD, SEM images, TG-DTA and water vapour adsorption isotherms.

AUTHOR INFORMATION

Corresponding Authors

Niket S. Kaisare – Department of Chemical Engineering, Indian Institute of Technology Madras, Chennai 600036, India
ORCID: 0000-0001-9395-8784
Email: nkaisare@iitm.ac.in

Stefan Kaskel - Chair of Inorganic Chemistry I, Technische Universität Dresden, Dresden 01069, Germany; Fraunhofer Institute for Material and Beam Technology (IWS), Dresden 01277, Germany
ORCID: 0000-0003-4572-0303
Email: stefan.kaskel@tu-dresden.de

Contributing Authors

Rimita Bose – Department of Chemical Engineering, Indian Institute of Technology Madras, Chennai 600036, India

Parasuraman Selvam – Department of Chemistry, Head of National Centre for Catalysis Research (NCCR), Indian Institute of Technology Madras, Chennai 600036, India
ORCID: 0000-0001-7807-2985
Volodymyr Bon – Chair of Inorganic Chemistry I, Technische Universität Dresden, Dresden 01069, Germany
ORCID: 0000-0002-9851-5031
Nadine Bönisch – Chair of Inorganic Chemistry I, Technische Universität Dresden, Dresden 01069, Germany

ACKNOWLEDGEMENT

N.S.K. and R.B. gratefully acknowledge financial support from Indian Institute of Technology Madras via the CCUS (CO_2 Capture, Utilization and Storage) Lab – An initiative supported under the Institute of Eminence (IoE) scheme of the Government of India. R.B. acknowledges financial support from the International Immersion Experience (IIE) Travel Award by IIT Madras for funding her research visit to TU Dresden. V.B. and S.K. acknowledge BMBF for financial support from the projects 05K22OD1, 05K22OD2 and DFG research unit MOF Switches (FOR2433).

REFERENCES

(1) Yaghi, O. M.; Li, H. Hydrothermal Synthesis of a Metal-Organic Framework Containing Large Rectangular Channels. *J. Am. Chem. Soc.* **1995**, *117* (41), 10401–10402.

(2) Furukawa, H.; Cordova, K. E.; O'Keeffe, M.; Yaghi, O. M. The Chemistry and Applications of Metal-Organic Frameworks. *Science (80-.).* **2013**, *341* (6149).

(3) Ding, M.; Cai, X.; Jiang, H.-L. Improving MOF Stability: Approaches and Applications. *Chem. Sci.* **2019**, *10* (44), 10209–10230.

(4) Horike, S.; Shimomura, S.; Kitagawa, S. Soft Porous Crystals. *Nat. Chem.* **2009**, *1* (9), 695–704.

(5) Kaur, J.; Kaur, G. Review on Flexible Metal-Organic Frameworks. *ChemistrySelect*

2021, *6* (32), 8227–8243.

(6) Tanaka, H.; Ohsaki, S.; Hiraide, S.; Yamamoto, D.; Watanabe, S.; Miyahara, M. T. Adsorption-Induced Structural Transition of ZIF-8: A Combined Experimental and Simulation Study. *J. Phys. Chem. C* **2014**, *118* (16), 8445–8454.

(7) Millange, F.; Walton, R. I. MIL-53 and Its Isoreticular Analogues: A Review of the Chemistry and Structure of a Prototypical Flexible Metal-Organic Framework. *Isr. J. Chem.* **2018**, *58* (9–10), 1019–1035.

(8) Horcajada, P.; Salles, F.; Wuttke, S.; Devic, T.; Heurtaux, D.; Maurin, G.; Vimont, A.; Daturi, M.; David, O.; Magnier, E.; Stock, N.; Filinchuk, Y.; Popov, D.; Riekel, C.; Férey, G.; Serre, C. How Linker's Modification Controls Swelling Properties of Highly Flexible Iron(III) Dicarboxylates MIL-88. *J. Am. Chem. Soc.* **2011**, *133* (44), 17839–17847.

(9) Siwaipram, S.; Bopp, P. A.; Keupp, J.; Pukdeejorhor, L.; Soetens, J.-C.; Bureekaew, S.; Schmid, R. Molecular Insight into the Swelling of a MOF: A Force-Field Investigation of Methanol Uptake in MIL-88B(Fe)–Cl. *J. Phys. Chem. C* **2021**, *125* (23), 12837–12847.

(10) Cao, Z.; Chen, L.; Li, S.; Yu, M.; Li, Z.; Zhou, K.; Liu, C.; Jiang, F.; Hong, M. A Flexible Two-Fold Interpenetrated Indium MOF Exhibiting Dynamic Response to Gas Adsorption and High-Sensitivity Detection of Nitroaromatic Explosives. *Chem. – An Asian J.* **2019**, *14* (20), 3597–3602.

(11) Mason, J. A.; Oktawiec, J.; Taylor, M. K.; Hudson, M. R.; Rodriguez, J.; Bachman, J. E.; Gonzalez, M. I.; Cervellino, A.; Guagliardi, A.; Brown, C. M.; Llewellyn, P. L.; Masciocchi, N.; Long, J. R. Methane Storage in Flexible Metal–Organic Frameworks with Intrinsic Thermal Management. *Nature* **2015**, *527* (7578), 357–361.

(12) Bolinois, L.; Kundu, T.; Wang, X.; Wang, Y.; Hu, Z.; Koh, K.; Zhao, D. Breathing-Induced New Phase Transition in an MIL-53(Al)–NH2 Metal–Organic Framework under High Methane Pressures. *Chem. Commun.* **2017**, *53* (58), 8118–8121.

(13) Hiraide, S.; Sakanaka, Y.; Kajiro, H.; Kawaguchi, S.; Miyahara, M. T.; Tanaka, H. High-Throughput Gas Separation by Flexible Metal–Organic Frameworks with Fast Gating and Thermal Management Capabilities. *Nat. Commun.* **2020**, *11* (1), 3867.

(14) Bondorf, L.; Fiorio, J. L.; Bon, V.; Zhang, L.; Maliuta, M.; Ehrling, S.; Senkovska, I.; Evans, J. D.; Joswig, J.-O.; Kaskel, S.; Heine, T.; Hirscher, M. Isotope-Selective Pore Opening in a Flexible Metal-Organic Framework. *Sci. Adv.* **2022**, *8* (15), eabn7035.

(15) Su, Y.; Otake, K.; Zheng, J.-J.; Horike, S.; Kitagawa, S.; Gu, C. Separating Water Isotopologues Using Diffusion-Regulatory Porous Materials. *Nature* **2022**, *611* (7935), 289–294.

(16) Freund, P.; Senkovska, I.; Kaskel, S. Switchable Conductive MOF–Nanocarbon Composite Coatings as Threshold Sensing Architectures. *ACS Appl. Mater. Interfaces* **2017**, *9* (50), 43782–43789.

(17) Freund, P.; Senkovska, I.; Zheng, B.; Bon, V.; Krause, B.; Maurin, G.; Kaskel, S. The Force of MOFs: The Potential of Switchable Metal–Organic Frameworks as Solvent Stimulated Actuators. *Chem. Commun.* **2020**, *56* (54), 7411–7414.

(18) Bon, V.; Krause, S.; Senkovska, I.; Grimm, N.; Wallacher, D.; Többens, D. M.; Kaskel, S. Massive Pressure Amplification by Stimulated Contraction of Mesoporous Frameworks**. *Angew. Chemie Int. Ed.* **2021**, *60* (21), 11735–11739.

(19) Park, K. S.; Ni, Z.; Côté, A. P.; Choi, J. Y.; Huang, R.; Uribe-Romo, F. J.; Chae, H. K.; O'Keeffe, M.; Yaghi, O. M. Exceptional Chemical and Thermal Stability of Zeolitic Imidazolate Frameworks. *Proc. Natl. Acad. Sci.* **2006**, *103* (27), 10186–10191.

(20) Aguado, S.; Bergeret, G.; Titus, M. P.; Moizan, V.; Nieto-Draghi, C.; Bats, N.; Farrusseng, D. Guest-Induced Gate-Opening of a Zeolite Imidazolate Framework. *New J. Chem.* **2011**, *35* (3), 546–550.

(21) Bennett, T. D.; Simoncic, P.; Moggach, S. A.; Gozzo, F.; Macchi, P.; Keen, D. A.; Tan, J.-C.; Cheetham, A. K. Reversible Pressure-Induced Amorphization of a Zeolitic Imidazolate Framework (ZIF-4). *Chem. Commun.* **2011**, *47* (28), 7983–7985.

(22) Hobday, C. L.; Bennett, T. D.; Fairen-Jimenez, D.; Graham, A. J.; Morrison, C. A.; Allan, D. R.; Düren, T.; Moggach, S. A. Tuning the Swing Effect by Chemical Functionalization of Zeolitic Imidazolate Frameworks. *J. Am. Chem. Soc.* **2018**, *140* (1), 382–387.

(23) Koutsianos, A.; Pallach, R.; Frentzel-Beyme, L.; Das, C.; Paulus, M.; Sternemann, C.;

Henke, S. Breathing Porous Liquids Based on Responsive Metal-Organic Framework Particles. *Nat. Commun.* **2023**, *14* (1), 4200.

(24) Lee, J. H.; Jeoung, S.; Chung, Y. G.; Moon, H. R. Elucidation of Flexible Metal-Organic Frameworks: Research Progresses and Recent Developments. *Coord. Chem. Rev.* **2019**, *389*, 161–188.

(25) McGuirk, C. M.; Runčevski, T.; Oktawiec, J.; Turkiewicz, A.; Taylor, M. K.; Long, J. R. Influence of Metal Substitution on the Pressure-Induced Phase Change in Flexible Zeolitic Imidazolate Frameworks. *J. Am. Chem. Soc.* **2018**, *140* (46), 15924–15933.

(26) Moggach, S. A.; Bennett, T. D.; Cheetham, A. K. The Effect of Pressure on ZIF-8: Increasing Pore Size with Pressure and the Formation of a High-Pressure Phase at 1.47 GPa. *Angew. Chemie Int. Ed.* **2009**, *48* (38), 7087–7089.

(27) Noguera-Díaz, A.; Villarroel-Rocha, J.; Ting, V. P.; Bimbo, N.; Sapag, K.; Mays, T. J. Flexible ZIFs: Probing Guest-Induced Flexibility with CO2, N2 and Ar Adsorption. *J. Chem. Technol. Biotechnol.* **2019**, *94* (12), 3787–3792.

(28) Huang, X.; Zhang, J.; Chen, X. [Zn(Bim)2] · (H2O)1.67: A Metal-Organic Open-Framework with Sodalite Topology. *Chinese Sci. Bull.* **2003**, *48* (15), 1531–1534.

(29) Zhao, P.; Fang, H.; Mukhopadhyay, S.; Li, A.; Rudić, S.; McPherson, I. J.; Tang, C. C.; Fairen-Jimenez, D.; Tsang, S. C. E.; Redfern, S. A. T. Structural Dynamics of a Metal–Organic Framework Induced by CO2 Migration in Its Non-Uniform Porous Structure. *Nat. Commun.* **2019**, *10* (1), 999.

(30) Arami-Niya, A.; Birkett, G.; Zhu, Z.; Rufford, T. E. Gate Opening Effect of Zeolitic Imidazolate Framework ZIF-7 for Adsorption of CH4 and CO2 from N2. *J. Mater. Chem. A* **2017**, *5* (40), 21389–21399.

(31) Wu, X.; Niknam Shahrak, M.; Yuan, B.; Deng, S. Synthesis and Characterization of Zeolitic Imidazolate Framework ZIF-7 for CO2 and CH4 Separation. *Microporous Mesoporous Mater.* **2014**, *190*, 189–196.

(32) Du, Y.; Mao, K.; Wooler, B.; Sharma, A. K.; Colmyer, D.; Nines, M.; Weston, S. C. Insights into the Flexibility of ZIF-7 and Its Structural Impact in Alcohol Adsorption. *J. Phys. Chem. C* **2017**, *121* (50), 28090–28095.

(33) Gücüyener, C.; van den Bergh, J.; Gascon, J.; Kapteijn, F. Ethane/Ethene Separation Turned on Its Head: Selective Ethane Adsorption on the Metal−Organic Framework ZIF-7 through a Gate-Opening Mechanism. *J. Am. Chem. Soc.* **2010**, *132* (50), 17704–17706.

(34) van den Bergh, J.; Gücüyener, C.; Pidko, E. A.; Hensen, E. J. M.; Gascon, J.; Kapteijn, F. Understanding the Anomalous Alkane Selectivity of ZIF-7 in the Separation of Light Alkane/Alkene Mixtures. *Chem. – A Eur. J.* **2011**, *17* (32), 8832–8840.

(35) Noguera-Díaz, A.; Bimbo, N.; Holyfield, L. T.; Ahmet, I. Y.; Ting, V. P.; Mays, T. J. Structure–Property Relationships in Metal-Organic Frameworks for Hydrogen Storage. *Colloids Surfaces A Physicochem. Eng. Asp.* **2016**, *496*, 77–85.

(36) Boutin, A.; Coudert, F.-X.; Springuel-Huet, M.-A.; Neimark, A. V; Férey, G.; Fuchs, A. H. The Behavior of Flexible MIL-53(Al) upon CH4 and CO2 Adsorption. *J. Phys. Chem. C* **2010**, *114* (50), 22237–22244.

(37) Hamon, L.; Llewellyn, P. L.; Devic, T.; Ghoufi, A.; Clet, G.; Guillerm, V.; Pirngruber, G. D.; Maurin, G.; Serre, C.; Driver, G.; van Beek, W.; Jolimaître, E.; Vimont, A.; Daturi, M.; Férey, G. Co-Adsorption and Separation of CO2−CH4 Mixtures in the Highly Flexible MIL-53(Cr) MOF. *J. Am. Chem. Soc.* **2009**, *131* (47), 17490–17499.

(38) Ichikawa, M.; Kondo, A.; Noguchi, H.; Kojima, N.; Ohba, T.; Kajiro, H.; Hattori, Y.; Kanoh, H. Double-Step Gate Phenomenon in CO2 Sorption of an Elastic Layer-Structured MOF. *Langmuir* **2016**, *32* (38), 9722–9726.

(39) Taylor, M. K.; Runčevski, T.; Oktawiec, J.; Bachman, J. E.; Siegelman, R. L.; Jiang, H.; Mason, J. A.; Tarver, J. D.; Long, J. R. Near-Perfect CO2/CH4 Selectivity Achieved through Reversible Guest Templating in the Flexible Metal–Organic Framework Co(Bdp). *J. Am. Chem. Soc.* **2018**, *140* (32), 10324–10331.

(40) Tian, T.; Wharmby, M. T.; Parra, J. B.; Ania, C. O.; Fairen-Jimenez, D. Role of Crystal Size on Swing-Effect and Adsorption Induced Structure Transition of ZIF-8. *Dalt. Trans.* **2016**, *45* (16), 6893–6900.

(41) Zhang, C.; Gee, J. A.; Sholl, D. S.; Lively, R. P. Crystal-Size-Dependent Structural Transitions in Nanoporous Crystals: Adsorption-Induced Transitions in ZIF-8. *J. Phys. Chem. C* **2014**, *118* (35), 20727–20733.

(42) Sakata, Y.; Furukawa, S.; Kondo, M.; Hirai, K.; Horike, N.; Takashima, Y.; Uehara, H.; Louvain, N.; Meilikhov, M.; Tsuruoka, T.; Isoda, S.; Kosaka, W.; Sakata, O.; Kitagawa, S. Shape-Memory Nanopores Induced in Coordination Frameworks by Crystal Downsizing. *Science (80-.).* **2013**, *339* (6116), 193–196.

(43) Hobday, C. L.; Krause, S.; Rogge, S. M. J.; Evans, J. D.; Bunzen, H. Editorial: The Influence of Crystal Size and Morphology on Framework Materials. *Front. Chem.* **2022**, *9*.

(44) Kavoosi, N.; Bon, V.; Senkovska, I.; Krause, S.; Atzori, C.; Bonino, F.; Pallmann, J.; Paasch, S.; Brunner, E.; Kaskel, S. Tailoring Adsorption Induced Phase Transitions in the Pillared-Layer Type Metal–Organic Framework DUT-8(Ni). *Dalt. Trans.* **2017**, *46* (14), 4685–4695.

(45) Abylgazina, L.; Senkovska, I.; Engemann, R.; Ehrling, S.; Gorelik, T. E.; Kavoosi, N.; Kaiser, U.; Kaskel, S. Impact of Crystal Size and Morphology on Switchability Characteristics in Pillared-Layer Metal-Organic Framework DUT-8(Ni). *Front. Chem.* **2021**, *9*.

(46) Krause, S.; Bon, V.; Senkovska, I.; Többens, D. M.; Wallacher, D.; Pillai, R. S.; Maurin, G.; Kaskel, S. The Effect of Crystallite Size on Pressure Amplification in Switchable Porous Solids. *Nat. Commun.* **2018**, *9* (1), 1573.

(47) Miura, H.; Bon, V.; Senkovska, I.; Ehrling, S.; Watanabe, S.; Ohba, M.; Kaskel, S. Tuning the Gate-Opening Pressure and Particle Size Distribution of the Switchable Metal–Organic Framework DUT-8(Ni) by Controlled Nucleation in a Micromixer. *Dalt. Trans.* **2017**, *46* (40), 14002–14011.

(48) Krause, S.; Bon, V.; Du, H.; Dunin-Borkowski, R. E.; Stoeck, U.; Senkovska, I.; Kaskel, S. The Impact of Crystal Size and Temperature on the Adsorption-Induced Flexibility of the Zr-Based Metal–Organic Framework DUT-98. *Beilstein J. Nanotechnol.* **2019**, *10*, 1737–1744.

(49) Ehrling, S.; Miura, H.; Senkovska, I.; Kaskel, S. From Macro- to Nanoscale: Finite Size Effects on Metal–Organic Framework Switchability. *Trends Chem.* **2021**, *3* (4), 291–304.

(50) Tu, M.; Wiktor, C.; Rösler, C.; Fischer, R. A. Rapid Room Temperature Syntheses of

Zeolitic-Imidazolate Framework (ZIF) Nanocrystals. *Chem. Commun.* **2014**, *50* (87), 13258–13260.

(51) Rodríguez-Carvajal, J. Recent Advances in Magnetic Structure Determination by Neutron Powder Diffraction. *Phys. B Condens. Matter* **1993**, *192* (1), 55–69.

(52) Boultif, A.; Louër, D. Powder Pattern Indexing with the Dichotomy Method. *J. Appl. Crystallogr.* **2004**, *37* (5), 724–731.

(53) Zhao, P.; Lampronti, G. I.; Lloyd, G. O.; Wharmby, M. T.; Facq, S.; Cheetham, A. K.; Redfern, S. A. T. Phase Transitions in Zeolitic Imidazolate Framework 7: The Importance of Framework Flexibility and Guest-Induced Instability. *Chem. Mater.* **2014**, *26* (5), 1767–1769.

(54) Tanaka, S.; Kida, K.; Okita, M.; Ito, Y.; Miyake, Y. Size-Controlled Synthesis of Zeolitic Imidazolate Framework-8 (ZIF-8) Crystals in an Aqueous System at Room Temperature. *Chem. Lett.* **2012**, *41* (10), 1337–1339.

(55) Jian, M.; Liu, B.; Liu, R.; Qu, J.; Wang, H.; Zhang, X. Water-Based Synthesis of Zeolitic Imidazolate Framework-8 with High Morphology Level at Room Temperature. *RSC Adv.* **2015**, *5* (60), 48433–48441.

(56) Phan, A.; Doonan, C. J.; Uribe-Romo, F. J.; Knobler, C. B.; O'Keeffe, M.; Yaghi, O. M. Synthesis, Structure, and Carbon Dioxide Capture Properties of Zeolitic Imidazolate Frameworks. *Acc. Chem. Res.* **2010**, *43* (1), 58–67.

(57) Cuadrado-Collados, C.; Fernández-Català, J.; Fauth, F.; Cheng, Y. Q.; Daemen, L. L.; Ramirez-Cuesta, A. J.; Silvestre-Albero, J. Understanding the Breathing Phenomena in Nano-ZIF-7 upon Gas Adsorption. *J. Mater. Chem. A* **2017**, *5* (39), 20938–20946.

(58) Van Vleet, M. J.; Weng, T.; Li, X.; Schmidt, J. R. In Situ, Time-Resolved, and Mechanistic Studies of Metal–Organic Framework Nucleation and Growth. *Chem. Rev.* **2018**, *118* (7), 3681–3721.

(59) Ohsaki, S.; Nakazawa, R.; Teranishi, A.; Nakamura, H.; Watano, S. Control of Gate Adsorption Characteristics of Flexible Metal-Organic Frameworks by Crystal Defect. *Microporous Mesoporous Mater.* **2020**, *302*, 110215.

(60) Krause, S.; Reuter, F. S.; Ehrling, S.; Bon, V.; Senkovska, I.; Kaskel, S.; Brunner, E.

Impact of Defects and Crystal Size on Negative Gas Adsorption in DUT-49 Analyzed by In Situ 129Xe NMR Spectroscopy. *Chem. Mater.* **2020**, *32* (11), 4641–4650.

(61) Yang, X.; Arami-Niya, A.; Xiao, G.; May, E. F. Flexible Adsorbents at High Pressure: Observations and Correlation of ZIF-7 Stepped Sorption Isotherms for Nitrogen, Argon, and Other Gases. *Langmuir* **2020**, *36* (49), 14967–14977.

(62) Du, Y.; Wooler, B.; Nines, M.; Kortunov, P.; Paur, C. S.; Zengel, J.; Weston, S. C.; Ravikovitch, P. I. New High- and Low-Temperature Phase Changes of ZIF-7: Elucidation and Prediction of the Thermodynamics of Transitions. *J. Am. Chem. Soc.* **2015**, *137* (42), 13603–13611.

(63) Fairen-Jimenez, D.; Moggach, S. A.; Wharmby, M. T.; Wright, P. A.; Parsons, S.; Düren, T. Opening the Gate: Framework Flexibility in ZIF-8 Explored by Experiments and Simulations. *J. Am. Chem. Soc.* **2011**, *133* (23), 8900–8902.

(64) Willems, T. F.; Rycroft, C. H.; Kazi, M.; Meza, J. C.; Haranczyk, M. Algorithms and Tools for High-Throughput Geometry-Based Analysis of Crystalline Porous Materials. *Microporous Mesoporous Mater.* **2012**, *149* (1), 134–141.

(65) Coudert, F.-X.; Jeffroy, M.; Fuchs, A. H.; Boutin, A.; Mellot-Draznieks, C. Thermodynamics of Guest-Induced Structural Transitions in Hybrid Organic−Inorganic Frameworks. *J. Am. Chem. Soc.* **2008**, *130* (43), 14294–14302.

(66) Watanabe, S.; Sugiyama, H.; Adachi, H.; Tanaka, H.; Miyahara, M. T. Free Energy Analysis for Adsorption-Induced Lattice Transition of Flexible Coordination Framework. *J. Chem. Phys.* **2009**, *130* (16), 164707.

(67) Evans, J. D.; Bon, V.; Senkovska, I.; Lee, H.-C.; Kaskel, S. Four-Dimensional Metal-Organic Frameworks. *Nat. Commun.* **2020**, *11* (1), 2690.

(68) Tanaka, S.; Fujita, K.; Miyake, Y.; Miyamoto, M.; Hasegawa, Y.; Makino, T.; Van der Perre, S.; Cousin Saint Remi, J.; Van Assche, T.; Baron, G. V; Denayer, J. F. M. Adsorption and Diffusion Phenomena in Crystal Size Engineered ZIF-8 MOF. *J. Phys. Chem. C* **2015**, *119* (51), 28430–28439.

(69) Liu, D.; Yan, L.; Li, L.; Gu, X.; Dai, P.; Yang, L.; Liu, Y.; Liu, C.; Zhao, G.; Zhao, X. Impact of Moderative Ligand Hydrolysis on Morphology Evolution and the

Morphology-Dependent Breathing Effect Performance of MIL-53(Al). *CrystEngComm* **2018**, *20* (15), 2102–2111.

(70) Sabetghadam, A.; Seoane, B.; Keskin, D.; Duim, N.; Rodenas, T.; Shahid, S.; Sorribas, S.; Guillouzer, C. Le; Clet, G.; Tellez, C.; Daturi, M.; Coronas, J.; Kapteijn, F.; Gascon, J. Metal Organic Framework Crystals in Mixed-Matrix Membranes: Impact of the Filler Morphology on the Gas Separation Performance. *Adv. Funct. Mater.* **2016**, *26* (18), 3154–3163.

(71) Keupp, J.; Schmid, R. Molecular Dynamics Simulations of the "Breathing" Phase Transformation of MOF Nanocrystallites. *Adv. Theory Simulations* **2019**, *2* (11), 1900117.

(72) Schaper, L.; Keupp, J.; Schmid, R. Molecular Dynamics Simulations of the Breathing Phase Transition of MOF Nanocrystallites II: Explicitly Modeling the Pressure Medium. *Front. Chem.* **2021**, *9*, 757680.

(73) Rogge, S. M. J.; Waroquier, M.; Van Speybroeck, V. Unraveling the Thermodynamic Criteria for Size-Dependent Spontaneous Phase Separation in Soft Porous Crystals. *Nat. Commun.* **2019**, *10* (1), 4842.

(74) Zhang, Y.; Wang, N.; Ji, S.; Zhang, R.; Zhao, C.; Li, J.-R. Metal–Organic Framework/Poly(Vinyl Alcohol) Nanohybrid Membrane for the Pervaporation of Toluene/n-Heptane Mixtures. *J. Memb. Sci.* **2015**, *489*, 144–152.

(75) Tang, Y.; Tanase, S. Water-Alcohol Adsorptive Separations Using Metal-Organic Frameworks and Their Composites as Adsorbents. *Microporous Mesoporous Mater.* **2020**, *295*, 109946.